PneuAct-II: Hybrid Manufactured Electromagnetically Stealth Pneumatic Stepper Actuator

Foad Sojoodi Farimani[1], Morteza Mojarradi[1], Edsko Hekman[1], and Sarthak Misra[1,2]

Abstract— Additive manufacturing (AM) is one of the emerging production methodologies transforming the industrial landscape. However, application of the technology in fluidic power transmission and actuation is still limited. AM pneumatic stepper motors have been previously introduced to the field of image-guided surgical robotics, where their disposability and customizability are considered a significant advantage over conventional manufacturing. However, intrinsic dimensional limitations of AM parts and their poor surface quality affect mechanical performance. In this study, a novel design, PneuAct-II, is presented combining AM, subtractive machining, and off-the-shelf components to achieve higher mechanical performance and resolution. Moreover, a motor identification setup has been built to automatically measure different aspects of the PneuAct motors, including wear, friction, leakage, and stall behavior at various boundary conditions. The effects of input pressure, stepping frequency, signal-width, and external torque on the stall behavior of motors with different clearances are studied. A maximum torque of $0.39\,\mathrm{N\cdot m}$ at an input pressure of $6.5\,\mathrm{bar}$ is achieved for a motor with a total volume of $90\,\mathrm{cm^3}$, and a clearance of $156\,\mathrm{\mu m}$. A nominal resolution of $2.25°$ at full-pitch and $1.125°$ at half-pitch is accomplished. Both resolution and mechanical performance ($667\,\mathrm{N\cdot m/(bar\cdot m^3)}$) outperform the state-of-the-art ($240\,\mathrm{N\cdot m/(bar\cdot m^3)}$) by PneuAct-I.

I. INTRODUCTION

Different industries prefer fluidic actuators (i.e., hydraulic and pneumatic) over conventional electromagnetic (EM) motors, due to their high mechanical output to size ratio, resilience towards harsh environments, and safety. For instance, being intrinsically non-electromagnetic, they do not require extensive shielding in explosive atmospheres. They can easily survive environments with high ionizing radiation (e.g., nuclear power-plants), high humidity, and in the presence of corrosive substances. Given the right materials and components (i.e., nonconductive and low magnetic susceptibility), fluidic actuators can be electromagnetically stealth. They can be used in sensitive environments such as the vicinity of
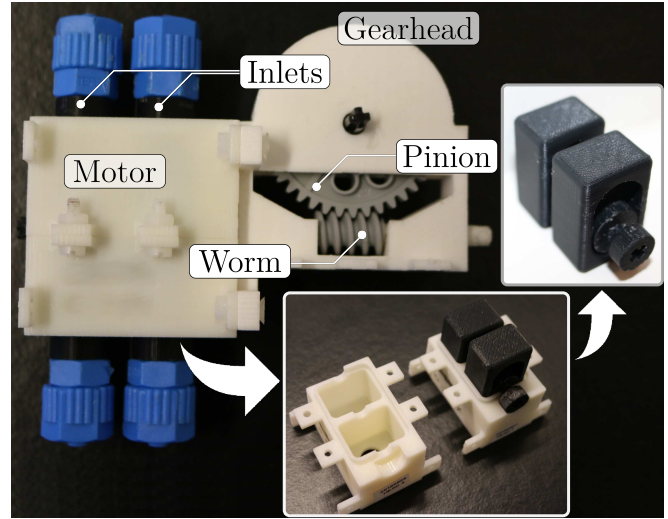
Fig. 1. A PneuAct-II actuation set including the motor and worm-pinion reduction drive [Fig. 2]. Two double-sided pistons, assembly-printed with the crankshaft, generate reciprocating motions following the pneumatic excitation patterns moderated by the Electro-Pneumatic Control Unit (EPCU) [Fig. 3]. The linear motion is consequently converted to rotation through the Scotch Yoke mechanism. The gear-head comprises a 3D printed body encompassing standard off-the-shelf LEGO® parts, together forming a slewing reduction drive of 40:1 ratio.

magnetic resonance (MR) imaging machines. In particular, pneumatic actuators have several advantages over hydraulics in image-guided minimally invasive interventions due to the fact that high pressurized air is abundantly available in hospitals, and possible leakages do not interfere with MR imaging nor hinders the safety of the operation [1].

Pneumatic actuators were introduced to the field of MR-guided robotic-assisted minimally invasive surgery by Hempel *et al.* in the form of conventional linear cylinder-pistons [2]. One major issue with the conventional pneumatic actuators is their unpredictable behavior, making position control challenging [3]. Air, being a compressible and viscous fluid, can behave chaotically when used as a power transmission medium, leading to uncontrollable overshoots if used in a robotic system [4]. Elhawary *et al.*, Tse *et al.*, and Chen *et al.* also presented rotational pneumatic motors using turbine or vane mechanisms [5]–[7]. Continuous fluidic actuators, volumetric or dynamic, offer higher speeds in comparison to stepper motors. However, implementing a reliable and accurate position control with continuous pneumatic actuators in the MR environment is difficult. Considering these limitations, several groups have been developing rotational fluidic stepper motors. Being limited state machines, stepper
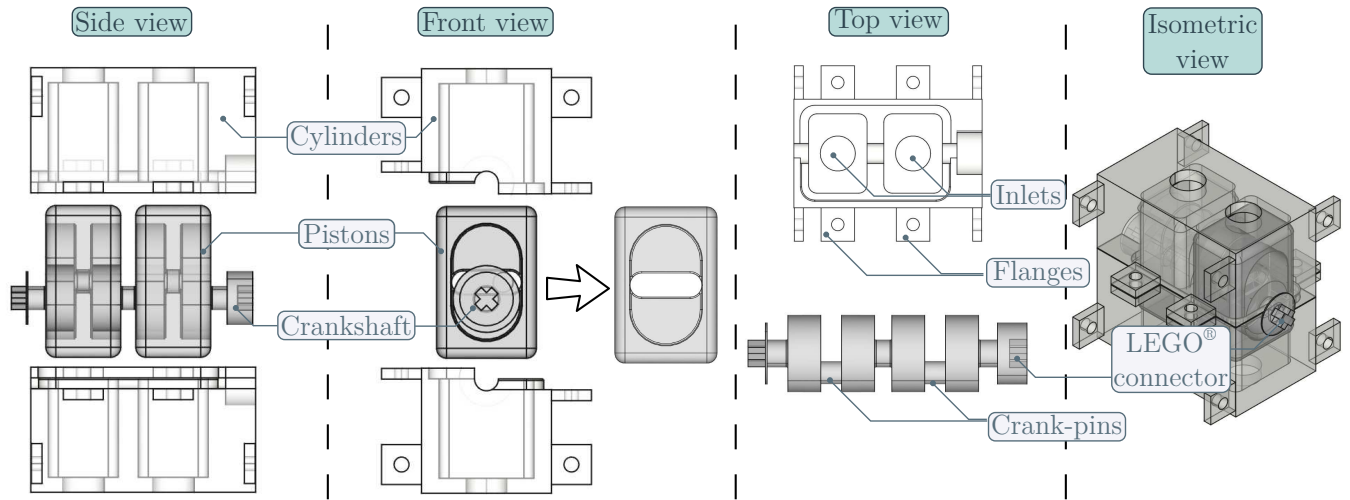
Fig. 2. Exploded and isometric views of the PneuAct-II motor designed in Free, Libre and Open Source CAD software FreeCAD. The motor comprises three different parts printed separately, including the two identical cylinder heads, and the assembly-printed combination of two pistons and the crankshaft. The shaft includes male and female standard plus-shaped (+) LEGO® connectors on both ends to account for modularity of the design. The two double-sided pistons constitute four chambers working like a four-piston engine, and the Scotch Yoke mechanism converts reciprocating motion to torque.

actuators have a more straightforward and reliable motion control than servo actuators, even in the absence of position feedback (i.e., open-loop control).

First mentions of fluidic stepper motors can be traced back to a patent by Musser at mid-nineteen-hundreds, inspired by his other invention, Harmonic Drive® [8]. Suzumori *et al.* were the first group to implement a rotational pneumatic stepper motor in the last decade of the 20th century [9]. However, the presented prototypes were not MR compatible. Taillant *et al.* demonstrated the first rotational MR-compatible pneumatic stepper motor for the light puncture robot (LPR) [10]. Stoianovici *et al.* reported a significant implementation of the concept, PneuStep actuator, used in the minimally invasive prostate intervention mechanism, MrBot [11]. Nonetheless, affordability and disposability required for a surgical setting, have not been taken into consideration. Slightam *et al.* and Wei *et al.* utilized additive manufacturing (AM) and non-assembly printing to develop pneumatic actuation in the form of a flexible chamber or turbine [12], [13]. However, the presented prototypes are not stepper actuators, requiring position feedback.

PneuAct-I was introduced as a fully 3D-assembly-printed pneumatic stepper actuator for the position control of robotic mechanisms in environments where EM motors are not permitted [14]. PneuAct-I aimed to be a paradigm shift in the field by providing a parametrically designed, affordable, disposable, recyclable, high resolution, safe (in terms of delivering passive backdrivability), high speed, and electro-magnetically stealth rotational pneumatic stepper actuator. Similarly, Boland *et al.* presented a fully AM rotational pneumatic stepper motor, with a maximum torque of $0.19\,\mathrm{N}\cdot\mathrm{m}$ and a speed of $2000\,\mathrm{RPM}$ at $6.2\,\mathrm{bar}$ input pressure, in a total volume of $512\,\mathrm{cm}^3$ [15]. Their prototype delivered a mechanical performance of $60\,\mathrm{N}\cdot\mathrm{m}/(\mathrm{bar}\cdot\mathrm{m}^3)$ and a raw resolution of $90°$. In comparison, PneuAct-I delivered a mechanical

performance of approximately $240\,\mathrm{N}\cdot\mathrm{m}/(\mathrm{bar}\cdot\mathrm{m}^3)$ (4 times higher) with a maximum holding torque of $0.14\,\mathrm{N}\cdot\mathrm{m}$, a resolution of $3°$ at an input pressure of $6.5\,\mathrm{bar}$ and an approximate total volume of $90\,\mathrm{cm}^3$.

However, more efficient actuators in same form-factor and price-range, could significantly improve the usability and application value. PneuAct-II is a major redesign of the rotational pneumatic stepper motors towards improving mechanical performance and resolution while sustaining the production costs and size minimal. To that end, a hybrid manufacturing methodology, CNC milling of the 3D-printed parts, is adopted to improve the surface quality of the AM parts in critical areas where friction and leakage are problematic. Injection-molded off-the-shelf LEGO® parts have been incorporated in the gear-box to deliver better performance while keeping costs as low as possible.

A motor identification setup is presented for the first time in the field, which is able to isolate and characterize different aspects of the pneumatic stepper motors, including internal friction, leakage, and stall behavior under various design and boundary conditions. The combination of hybrid manufactured pneumatic stepper motor, PneuAct-II, and the gear-head reduction drive, is able to sustain a maximum stall torque of $0.39\,\mathrm{N}\cdot\mathrm{m}$ at an input pressure of $6.5\,\mathrm{bar}$, delivering 2.7 times better mechanical performance than the previous version. A resolution of $2.25°$ at the full-pitch drive and $1.125°$ at half-pitch is delivered, which are improvements over the latest records in the field.

II. Materials and Methods

Every PneuAct-II actuation set contains two main sections, the mechanical modules, including the gear-head and motor itself, and the electro-pneumatic control unit (EPCU). In the following paragraphs, these sections, their submodules, relationship and functionalities are described:
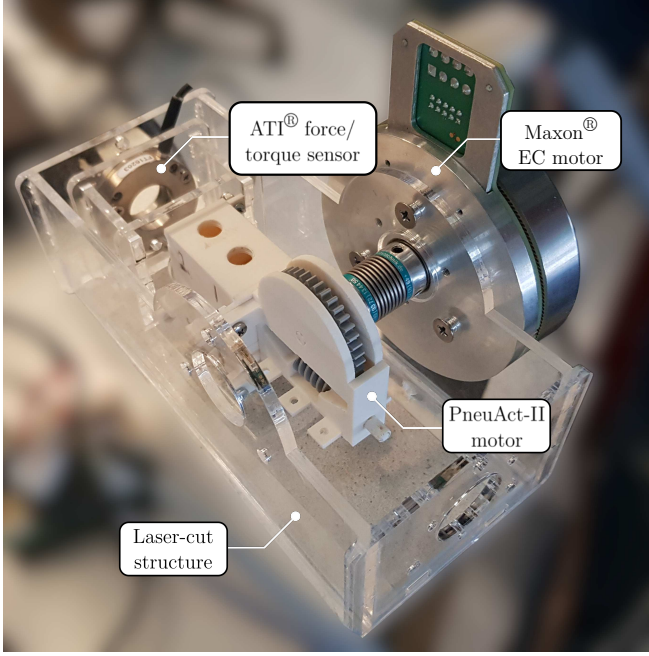
Fig. 3. A schematic diagram of the electro-pneumatic control unit (EPCU) and the motor identification setup: The EPCU is responsible for generating the square wave excitation signals controlling the pneumatic valves. It also controls the pressure regulator while reading the airflow rates from the flow-meter. Different parameters, including the input pressure, duty-cycle, and the stepping frequency, can be controlled directly from the LabVIEW® GUI or manually from the boards using the potentiometers and switches. The motor identification setup includes the Maxon® EC motor, which sends and receives data from the computer through the driver, and the Nano43® sensor sends six values (three forces and three torques) to the computer through the Netbox.

A. Mechanical Design

The mechanical section of the PneuAct-II actuator consists of two modules, the motor itself and the gear-head:

1) Motor: PneuAct-II employs a Scotch Yoke mechanism (or slotted link mechanism), to convert the reciprocating motion of the pistons to rotation [Fig. 2]. The mechanism is kinematically analogous to PneuAct-I, except in the new version the two double-acting cylinders-pistons offer four steps-per-revolution, instead of three one-sided pistons [14]. PneuAct-II has a better raw resolution than the previous generation as it has a step-size of $90°$ at full-pitch instead of $120°$ previously reported and a half-pitch step-size of $45°$ instead of $60°$.

The motor comprises four parts printed in three components, including the two identical segments of the cylinder-heads, and the assembly-printed combination of the crank-shaft plus two pistons [Fig. 2]. The crank-shaft has two off-centric crank-pins with a $90°$ degrees phase-shift, which slide in the slotted body of the pistons. Pistons are actuated through the excitation pressure signal (i.e., square wave signal) generated by the EPCU. The parts are 3D printed with a Stratasys® (Rehovot, Israel) Fortus-250mc® machine using ABSplus-P430® material with a nominal layer thickness of $0.1778\,\text{mm}$. To improve energy efficiency, reducing leakage and friction, cylinder heads are machined with different clearances $100\,\mu\text{m}$ to $250\,\mu\text{m}$. PneuAct-II is designed with modularity in mind. The standard plus-shaped (+) LEGO® (Billund, Denmark) connector is placed at both sides of the motor and the gear-head. It means several motors can be put in series to improve resolution and torque. The connection can also be used for mounting the gear-head, position encoder, torque sensor, and clutch/brake.

2) Gear-head: In PneuAct-I, the entire gear-head was 3D-printed to achieve high affordability and customizability. However, for non-assembly-printing with a Fortus-250mc®

printer, a small gap of $0.3\,\text{mm}$ needs to be included between adjacent surfaces, to avoid interfusion. Not only the gap can introduce some backlash, but also it may result in some actuation steps being skipped at high external torques — this affects both the mechanical performance and the actuator's accuracy. Furthermore, the fused deposition modeling (FDM®) manufactured parts suffer from an inferior surface quality (in comparison to other AM methods). As a result, the fully FDM® manufactured assembly-printed gear-head delivered a low energy efficiency and poor determinism.

In PneuAct-II, the gear-head comprises a 3D-printed body which encompasses off-the-shelf injection molded parts with better dimensional accuracy and surface quality. A worm-pinion reduction drive of $40{:}1$ gear-ratio (similar to the one used for PneuAct-I), has been developed, except here LEGO® gear-pinion (part numbers 3649 and 4716) have been used to improve energy efficiency and alleviate backlash/play. A nominal final resolution of $2.25°$ at full-pitch and $1.125°$ at half-pitched is achieved, which are improvements over $3°$ and $1.5°$ of PneuAct-I.

B. Electro-Pneumatic Control Unit (EPCU)

EPCU is responsible for generating the square wave signal, controlling solenoid pneumatic valves, given the duty-cycle (or signal width) and stepping frequency. The amplitude of the pneumatic waves is modulated via a Festo® (Esslingen, Germany) VPEE pressure regulator ($2\,\text{bar}$ to $7.5\,\text{bar}$). Rotational direction (i.e., clockwise or counterclockwise) and control mode (position and speed) can be selected using on-board switches. The ECPU also reads the flow from a Festo® SFAB sensor. The above parameters can be controlled via physical knobs (potentiometers) and switches on the electronic board or via the LabVIEW® (National Instruments™: Austin, United States) graphical user interface on the computer, through serial communication.

Fig. 4. The motor identification setup comprises a 6-DOF force/torque sensor, a Maxon® EC motor with torque and speed control. The laser-cut structure encompasses the PneuAct-II motor and the gear-head. The Maxon® motor can be mounted to the motor's shaft or the gear-box output for different phases of the experiments.

C. Motor Identification Setup

In previous studies, two different methods were used to measure the output torque of the motors. The first method is to use a cable and pulley coupled rotationally to the output shaft of the motors to lift some weights or deform an energy storage compliant component (i.e., spring). Another approach is to use dynamometers, which measure the instantaneous exerted power of the motors. In this study, a motor identification setup has been made to measure different aspects of the PneuAct-II motor [Fig. 4]. The setup comprises a Maxon® (Friedrichsdorf, Germany) EC motor, an ATI® (NC, USA) 6-DOF force/torque (F/T) sensor, and a laser-cut mechanical structure encompassing the PnauAct-II motor. The Maxon® motor can be torque or velocity controlled at different phases of the experiments while data is being collected from the F/T sensor, EM motor's driver, and EPCU.

III. EXPERIMENTS AND RESULTS

Several experiments are designed to isolate and characterize different properties of the PneuAct-II motors, identifying the stall points at various boundary conditions. Initially, the freshly 3D-printed motor and the gear-head are placed in the experimental setup, and the Maxon® motor rotates them through the worm-gear shaft at a constant speed. The required torque is recorded though both the EM motor's encoder and the F/T sensor. Changes of the torque over time, represent wear in the motor and gear-head. This experiment is continued until the torque asymptotes to a constant value, indicating that wear has stabilized.

Consequently, to identify the stall behavior of the PneuAct motors, they are actuated at different speeds (i.e., stepping

frequencies), duty-cycles, and input pressures while the external torque is applied up to a maximum of $0.5\,\mathrm{N}\cdot\mathrm{m}$ [Fig. 9]. Position of the motors is recorded throughout the experiments. The experiment are repeated for different boundary conditions: stepping frequencies ($1\,\mathrm{Hz}$ to $25\,\mathrm{Hz}$), duty-cycles ($25\,\%$, $50\,\%$, $75\,\%$ and $100\,\%$), and input pressures ($2\,\mathrm{bar}$ to $7.5\,\mathrm{bar}$). Experiments are conducted on machined motors with different clearances ($120\,\mu\mathrm{m}$ to $270\,\mu\mathrm{m}$). Figures 5 to 8 show the bootstrapped results of the above experiments for a PneuAct-II motor with a piston dimension of 15×20 mm, and a stroke length of $8\,\mathrm{mm}$. [1]

Figure [5] shows the average behavior of the stall torque at different input pressures. The minimum required pressure for actuating the motor is approximately $3\,\mathrm{bar}$, which is to overcome internal friction in the system. The overall relationship is proportional, which is in agreement with the simplified energy equilibrium equation describing the average dynamic behavior of the system:

$$\tilde{\tau}\tilde{\omega} < \tilde{P}\tilde{Q}\,, \tag{1}$$

where

$\tilde{P} =$ Average input pressure (bar)
$\tilde{\tau} =$ Average external torque ($\mathrm{N}\cdot\mathrm{m}$)
$\tilde{\omega} =$ Average angular speed ($\mathrm{rad/s}$)

and $\tilde{Q}$ is the average air flow in ($\mathrm{m^3/s}$) calculated as:

$$\tilde{Q} = V_0 n \frac{\tilde{\omega}}{2\pi}\,, \tag{2}$$

and

$V_0 =$ is the maximum volume of the chamber ($\mathrm{m^3}$)
$n\ \ =$ number of cylinders (4 for PneuAct-II)

Substituting $\tilde{Q}$ from eq. (2) in eq. (1) and omitting $\tilde{\omega}$ from both sides shows that the stall behavior should be independent of speed or stepping frequency ($f_s = n\omega/2\pi$).

Figure [6] illustrates the overall relationship between the stall torque and stepping frequency at different input pressures. The significance of the graph is to demonstrate the above prediction that the stall torque does not theoretically depend on the rotational speed of the motor. This is, of course, contradicting previous studies, where a negative relationship between stall torque and rotational speed had been reported. As eqs. (1) and (2) show if the effect of speed on leakage and friction are neglected, the stall torque should be independent of the motor's frequency. The reason previous studies, including the study done by the authors [14], have identified a negative relationship between stall torque and stepping frequency can actually be attributed to the fact that a constant duty-cycle has been maintained throughout the experiments. Hence, higher frequencies lead to smaller signal-width, and less energy is pumped to the motors.

The solenoid valves have a rise-time and minimum pilot pressure, required to overcome their internal static friction.

---

[1] experimental data and analysis code can be acquired at GitHub repository http://bit.ly/2kr1rf3
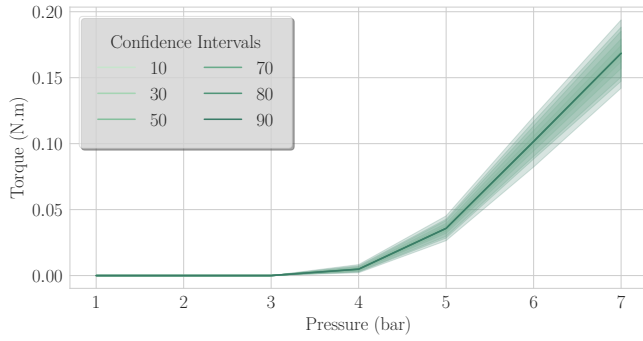
Fig. 5. Bootstrapped stall torque is plotted at various input pressure contoured with different confidence intervals. A linear relationship can be observed as predicted by eq. (1) while an average minimum pressure of 3 bar is required to overcome internal friction and leakage.
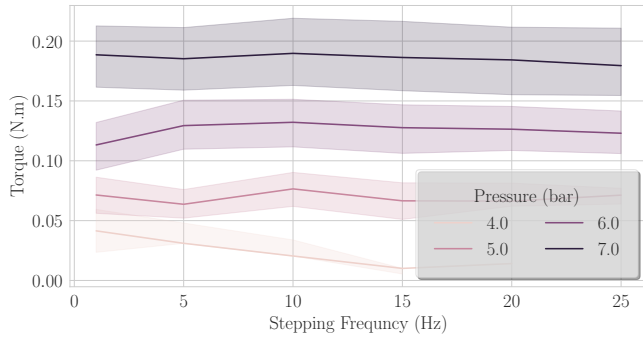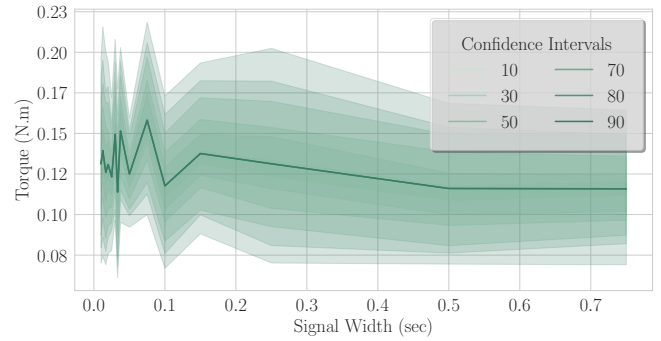

Fig. 7. The stall torque is plotted against signal-width, contoured at different confidence intervals. The plot demonstrates that the stall behavior is independent of the signal-width while it is above a certain threshold. The PneuAct motor behaves chaotically when signal-widths is below the said threshold due to the vales rise time as well as their minimum pilot pressure.

Fig. 6. Stall torque versus stepping frequency is plotted at various input pressures with a confidence interval of 50%. No significant relationship between torque and stepping frequency (i.e., rotational speed) is observed.
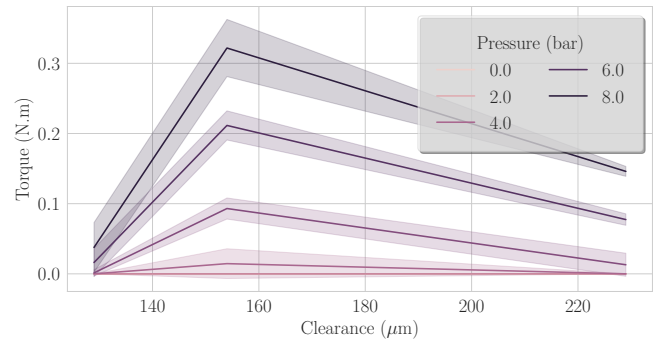

Fig. 8. The stall torque is plotted for motors with various clearances (i.e., average gap size between the perimeter of the pistons and the cylinder) at different input pressures. The error bands width is the standard deviation. The plot demonstrates interaction between leakage and friction at different clearances, showing optimum performance at $150\,\mu m$.

Additionally, propagation of the pressure signals through the tubing causes both delay and dissipation, as presented in the previous study [14]. As a result, signal-widths and pressures below certain thresholds lead to an unstable behavior of the valves. This can be seen in [Fig. 7] where signal-widths below $9\,ms$ result in somewhat unstable behavior.

Figure [8] shows the stall torque of the motors with different clearances at various input pressures. This graph represents the trade-off between friction and leakage in PnuAct-II actuators. At smaller gap sizes, the normal force between two sliding surfaces increases friction while increasing the clearance would rise leakage. As a result, there is an optimum clearance where the energy efficiency of the PneuAct motor is at its maximum. The optimum clearance, as measured in the experiments, is approximately $150\,\mu m$, which is in agreement with the value reported in the previous study by the authors for fully 3D-printed motors [14].

One significant observation in this study was the inverse motion of the motors in certain conditions. The worm-pinion reduction-derives are usually self-locking; hence, the external torque on the pinion's shaft should not be able to rotate the gearbox in the opposite direction. However, during the experiments, a negative rotation in the PneuAct motor was observed [Fig. 9]. Further investigation revealed that this behavior can be attributed to the stall phenomenon. Basically, when the PneuAct motor experiences a stall, some steps are

skipped. As a result, while the crank-pin is in the wrong position, the following steps can rotate the motor in the opposite direction where there is no opposing potential.

It was previously presumed that pneumatic stepper motors, in contrast to continuous actuators, can deliver a relatively precise position control in an open-loop configuration. This was considered as an advantage over the servo actuators such as turbines and vane motors. However, this observation implies that even the stepper motors require a position encoder if a safe and reliable position control (highly required in a surgical application) should be expected.

IV. CONCLUSIONS

In this study, a major redesign of 3D-printed and parametrically designed pneumatic stepper motors is introduced. A hybrid manufacturing approach is employed where the cylinders are machined to alleviate leakage and friction. A new mechanical design with two double-acting cylinder-pistons is presented to improve machinability, resolution, and backlash. In comparison to PneuAct-I, the new version generates 2.7 times higher mechanical performance, while keeping the production time/costs minimal. The new version has a better resolution of $2.25°$ at full-pitch, breaking the previous record in the field by PneuAct-I, and a resolution of
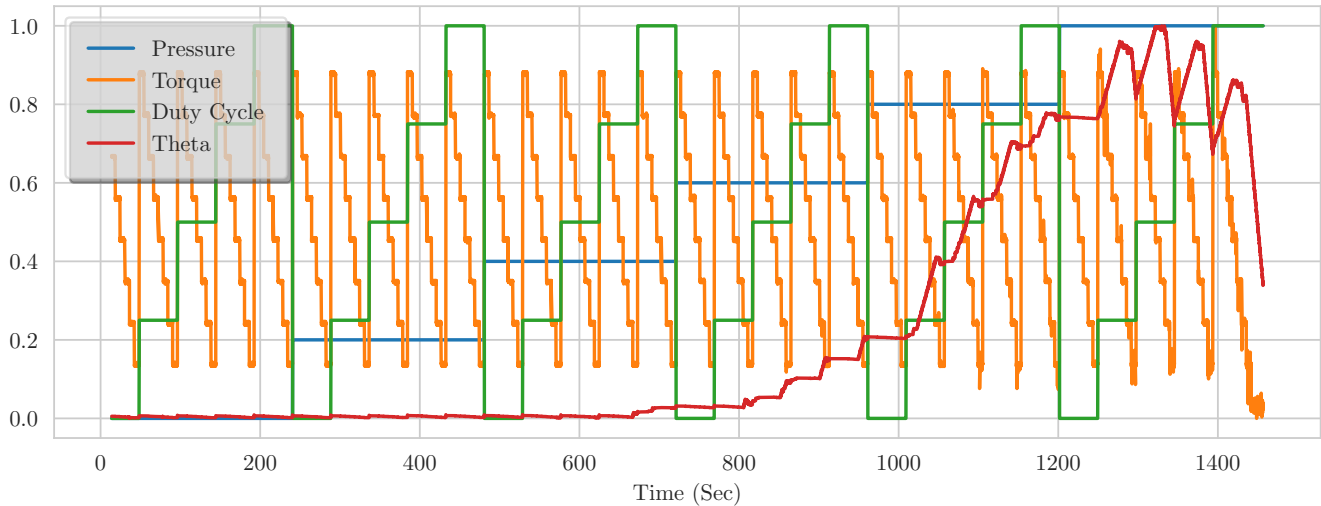
Fig. 9. The stall behavior of a PneuAct-II in Step 1. of Phase3., in a sample with a clearance of $224\,\mu m$ at various input pressures, external torques, and duty-cycles is illustrated in a normalized plot. Constant Theta (i.e., position) represent stall of the PneuAct actuator. In certain conditions, especially at high pressures, the PneuAct motor rotates in the opposite direction (i.e., reducing Theta) due to the missing-steps phenomenon, as explained in the text.

$1.125°$ at half-pitch. It was shown that there is no significant relation between stall torque and stepping frequency as far as the signal-width is above a certain threshold determined by the rise time of the solenoid valves, dimension (length and diameter) of the pneumatic tubes. Although this is in contrast to the previous studies, it is in agreement with the more accurate mathematical model.

A motor identification setup, comprising a 6-DOF force/torque sensor and an EM stepper motor with speed and torque-control, is developed to measure different aspects of the PneuAct-II motor. The setup is able to measure internal friction, pneumatic efficiency, minimum required signal-width at specific input pressure and external torque, and stall torque at specific input pressure and stepping frequency. This allowed measuring aspects of the pneumatic stepper motor, which were not possible with the conventional methods. This study also demonstrated that backdrivable pneumatic stepper motors might not deliver a reliable position control in an open-loop configuration, concluding that encoders are necessary for safety. A follow-up work for this project could be to develop such an encoder based on a similar design rationale and manufacturing principles.

REFERENCES

[1] H. Elhawary, A. Zivanovic, B. Davies, and M. Lampérth, "A review of magnetic resonance imaging compatible manipulators in surgery," *Proceedings of the Institution of Mechanical Engineers, Part H: Journal of Engineering in Medicine*, vol. 220, pp. 413–424, mar 2006.

[2] E. Hempel, H. Fischer, L. Gumb, T. Höhn, H. Krause, U. Voges, H. Breitwieser, B. Gutmann, J. Durke, M. Bock, and A. Melzer, "An MRI-compatible surgical robot for precise radiological interventions," *Computer Aided Surgery*, vol. 8, no. 4, pp. 180–191, 2003.

[3] G. S. Fischer, I. Iordachita, C. Csoma, J. Tokuda, S. P. DiMaio, C. M. Tempany, N. Hata, and G. Fichtinger, "MRI-compatible pneumatic robot for transperineal prostate needle placement," *IEEE/ASME Transactions on Mechatronics*, vol. 13, pp. 295–305, jun 2008.

[4] D. Comber and E. J. Barth, "Precision position tracking of MR-compatible pneumatic piston-cylinder using sliding mode control," in *ASME 2011 Dynamic Systems and Control Conference and Bath/ASME Symposium on Fluid Power and Motion Control, Volume 1*, pp. 45–51, ASMEDC, jan 2011.

[5] H. Elhawary, A. Zivanovic, M. Rea, Z. T. H. Tse, D. McRobbie, I. Young, M. Paley, B. Davies, and M. Lampérth, "A MR compatible mechatronic system to facilitate magic angle experiments in vivo," in *Medical Image Computing and Computer-Assisted Intervention – MICCAI 2007*, (Berlin, Heidelberg), pp. 604–611, Springer, 2007.

[6] Z. T. H. Tse, H. Elhawary, A. Zivanovic, M. Rea, M. Paley, G. Bydder, B. L. Davies, I. Young, and M. U. LampÉrth, "A 3-DOF MR-compatible device for magic angle related in vivo experiments," *IEEE/ASME Transactions on Mechatronics*, vol. 13, pp. 316–324, June 2008.

[7] Y. Chen, A. Squires, R. Seifabadi, S. Xu, H. K. Agarwal, M. Bernardo, P. A. Pinto, P. Choyke, B. Wood, and Z. T. H. Tse, "Robotic system for MRI-guided focal laser ablation in the prostate," *IEEE/ASME Transactions on Mechatronics*, vol. 22, pp. 107–114, Feb 2017.

[8] W. Musser, "Fluid wave generator for harmonic drive," may 7 1963. U.S. Patent 3088333.

[9] K. Suzumori, K. Hori, and T. Miyagawa, "A direct-drive pneumatic stepping motor for robots: designs for pipe-inspection microrobots and for human-care robots," in *Proc. IEEE Int. Conf. on Robotics and Automation (ICRA)*, vol. 4, pp. 3047–3052, May 1998.

[10] E. Taillant, J.-C. Avila-Vilchis, C. Allegrini, I. Bricault, and P. Cinquin, "CT and MR Compatible Light Puncture Robot: Architectural Design and First Experiments," in *Medical Image Computing and Computer-Assisted Intervention – MICCAI 2004*, (Berlin, Heidelberg), pp. 145–152, Springer, 2004.

[11] D. Stoianovici, A. Patriciu, D. Petrisor, D. Mazilu, and L. Kavoussi, "A new type of motor: Pneumatic step motor," *IEEE/ASME Transaction on Mechatronics*, vol. 12, pp. 98–106, Feb 2007.

[12] J. E. Slightam and V. R. Gervasi, "Novel integrated fluid-power actuators for functional end-use components and systems via selective laser sintering nylon," in *23rd Ann Int Solid Freeform Fabrication Symp*, pp. 197–211, 2012.

[13] Y. Wei, Y. Chen, Y. Yang, and Y. Li, "Novel design and 3D printing of nonassembly controllable pneumatic robots," *IEEE/ASME Transactions on Mechatronics*, vol. 21, pp. 649–659, April 2016.

[14] F. Sojoodi Farimani and S. Misra, "Introducing PneuAct: Parametrically-Designed MRI-Compatible Pneumatic Stepper Actuator," in *Proc. IEEE Int. Conf. on Robotics and Automation (ICRA)*, (Brisbane, Australia), pp. 200–205, May 21-25 2018. https://goo.gl/9o2p6u.

[15] B. L. Boland, S. Xu, B. Wood, and Z. T. H. Tse, "High speed pneumatic stepper motor for mri applications," *Annals of Biomedical Engineering*, vol. 47, pp. 826–835, Mar 2019.